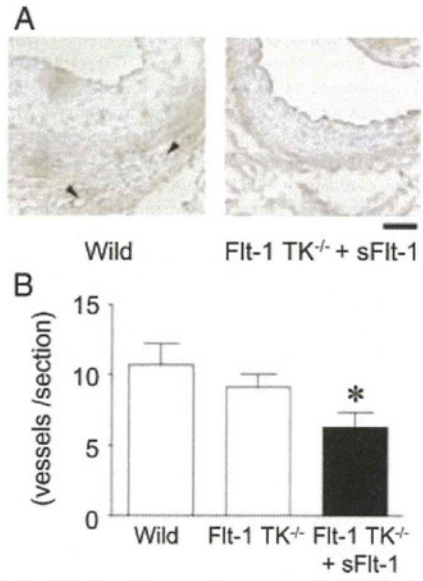

Figure 5. Adventitial angiogenesis was evaluated by CD31 immunostaining 28 days after wire injury (A). sFlt-1 gene transfer into Flt-1 $TK^{-/-}$ mice inhibited adventitial angiogenesis compared with wild mice (B). n=7 for each group. *$P<0.05$ versus wild type.

Effect of sFlt-1 Gene Transfer on Adventitial Angiogenesis

Adventitial angiogenesis was evaluated by counting CD31-positive endothelial cells in the adventitia of injured femoral arteries. Adventitial angiogenesis was equivalent in WT and Flt-1 $TK^{-/-}$ mice, however, was significantly decreased in Flt-1 $TK^{-/-}$ mice after sFlt-1 gene transfer compared with WT mice (Figure 5).

Discussion

In this study, we aimed to clarify the relative importance of 2 VEGF receptors, flt-1 and flk-1/KDR in neointima formation after intraluminal wire injury. Major findings were: (1) Flt-1 TK deficiency unaffected neointima formation, (2) sFlt-1 gene transfer into Flt-1 $TK^{-/-}$ mice remarkably suppressed neointima formation, and (3) VEGF induced MCP-1 expression in VSMCs which was blocked by flk-1–specific antibody. The inhibition of neointima formation by flk-1 blockade was preceded by significant reduction of MCP-1 expression in the medial VSMCs 3 days after injury, and monocyte infiltration, VSMC proliferation, and perivascular neovascularization 7 days after injury. These in vivo results suggest that flk-1 plays a primary role in the development of neointima by regulating macrophage-mediated inflammation in this model.

Inflammation in the vascular wall, mainly mediated by monocyte and macrophage, is a hallmark of vascular remodeling after injury as evident in our previous studies using cuff injury in mice and balloon injury in rats, rabbits, and monkeys, in which MCP-1 blockade effectively suppresses vascular inflammation and remodeling.[24–26] It is reported that VEGF induces MCP-1 expression in endothelial cells[27]; in turn, MCP-1 induces VEGF in VSMCs.[28] Macrophage-mediated inflammation activates VSMC migration and proliferation by cytokines, or by redox-dependent signaling.[29,30]

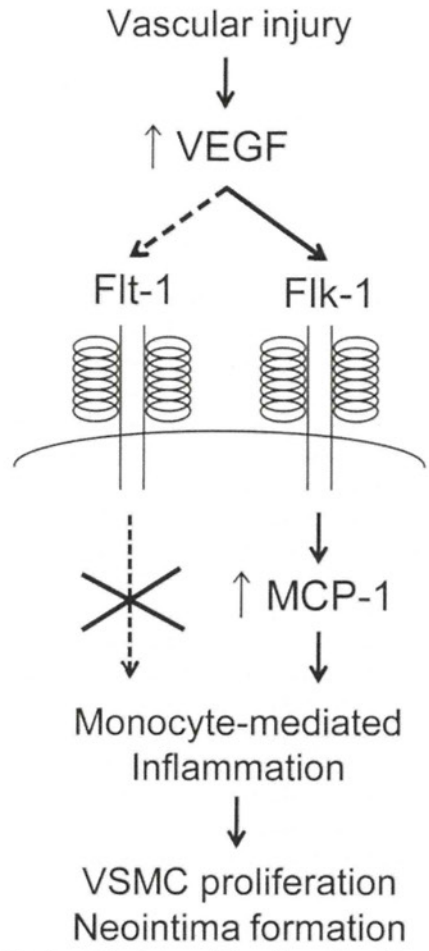

Figure 6. Flk-1 accelerates neointima formation after vascular injury. VEGF is upregulated in vascular wall cells after wire injury. VEGF activates flk-1 to cause MCP-1 induction and monocyte recruitment to the injured vascular wall. Monocyte/macrophage-mediated inflammation results in VSMC proliferation and neointima formation. Flt-1–mediated monocyte chemotaxis is minor to cause neointima formation in vivo, as indicated by dotted lines.

Although flk-1 is expressed mainly in endothelial cells, VSMCs also express flk-1,[31] and the present study revealed a new mechanism that flk-1 mediates MCP-1 expression in VSMCs and monocyte recruitment after injury. This VEGF/MCP-1–positive feedback and downstream signaling is considered to be a major underlying mechanism in neointima formation after injury, as shown in our previous studies using sFlt-1 and MCP-1 mutant[19,24–26] (Figure 6).

It has been reported that VEGF induces direct macrophage chemotaxis by flt-1–mediated mechanisms, whereas flk-1 is not expressed on monocytes/macrophages.[13] Indeed, Flt-1 TK deficiency abrogated VEGF-induced chemotaxis in peritoneal macrophages in the present study; however, Flt-1 TK deficiency had no effect on macrophage infiltration into injured arterial wall and neointima formation in in vivo setting. In the present study, blockade of flk-1 inhibited MCP-1 expression in the medial VSMCs and abrogated monocyte accumulation in the vascular wall after injury. Thus, we considered that MCP-1, which is regulated by VEGF/flk-1 pathway, mainly mediates macrophage chemo-

taxis rather than VEGF/flt-1 expressed on monocyte itself. This mechanism well explains the in vivo effect of flk-1 blockade on monocyte accumulation after injury.

In the present study, sFlt-1 gene transfer also inhibited adventitial angiogenesis after injury. Inhibition of adventitial angiogenesis may be another mechanism by which flk-1 blockade inhibits neointima formation, because a positive correlation was observed between adventitial blood vessel formation and neointima formation in various injury model including rabbit collar placement model.[32]

The role of VEGF in neointima formation may be different depending on the mode of injury or the species studied. For example, Isner et al[33] reported that local delivery of VEGF accelerates reendothelialization and attenuates intimal hyperplasia in balloon-injured rat carotid artery. Hutter et al[5] reported in mouse wire injury model that intravenous injection of VEGF adenovirus promoted endothelial repair and inhibited neointima formation. By contrast, Khurana et al[32] reported that adenovirus-mediated VEGF gene transfer exacerbates adventitial neovascularization and neointima formation in rabbit periadventitial collar replacement model, which was abrogated by administration of sFlt-1. Thus, there remain controversies in the role of VEGF gene transfer per se in neointima formation in previous studies. In the present study, we administered sFlt-1 plasmid intramuscularly, and sFlt-1, which was detected in the serum, blocked VEGF signaling at the site of vascular injury. In our previous study, we have reported that reendothelialization is complete 14 days after wire injury in mice irrespective of VEGF blockade by sFlt-1 gene transfer.[2] Thus, it is suggested that on complete reendothelialization, excess VEGF may accelerate neointima formation by promoting monocyte-mediated inflammation through flk-1–dependent MCP-1 expression in the injured vascular wall at least in the murine wire injury model studied. In this situation, Flk-1–specific VEGF blockade may be another potential approach to control vascular inflammation and subsequent remodeling after injury.

In conclusion, the present study demonstrated that soluble sFlt-1 gene transfer ameliorates neointima formation after wire injury in flt-1 tyrosine kinase–deficient mice by inhibiting MCP-1 expression in the medial VSMCs and resulting monocyte-mediated inflammation. The present findings suggest that endogenous VEGF accelerates neointima formation after injury through flk-1–dependent mechanisms, and provide new insights into complex VEGF-mediated signaling in vascular remodeling.

Sources of Funding

This study was supported by Grants-in-Aid for Scientific Research (19390216, 19650134) from the Ministry of Education, Science, and Culture, Tokyo, Japan and by Health Science Research Grants (Research on Translational Research and Nano-medicine) from the Ministry of Health Labor and Welfare, Tokyo, Japan.

Disclosures

None.

References

1. Brasen JH, Kivela A, Roser K, Rissanen TT, Niemi M, Luft FC, Donath K, Yla-Herttuala S. Angiogenesis, vascular endothelial growth factor and platelet-derived growth factor-BB expression, iron deposition, and oxidation-specific epitopes in stented human coronary arteries. *Arterioscler Thromb Vasc Biol.* 2001;21:1720–1726.
2. Ohtani K, Egashira K, Hiasa K, Zhao Q, Kitamoto S, Ishibashi M, Usui M, Inoue S, Yonemitsu Y, Sueishi K, Sata M, Shibuya M, Sunagawa K. Blockade of vascular endothelial growth factor suppresses experimental restenosis after intraluminal injury by inhibiting recruitment of monocyte lineage cells. *Circulation.* 2004;110:2444–2452.
3. Shibata M, Suzuki H, Nakatani M, Koba S, Geshi E, Katagiri T, Takeyama Y. The involvement of vascular endothelial growth factor and flt-1 in the process of neointimal proliferation in pig coronary arteries following stent implantation. *Histochem Cell Biol.* 2001;116:471–481.
4. Zhao Q, Egashira K, Hiasa K, Ishibashi M, Inoue S, Ohtani K, Tan C, Shibuya M, Takeshita A, Sunagawa K. Essential role of vascular endothelial growth factor and Flt-1 signals in neointimal formation after periadventitial injury. *Arterioscler Thromb Vasc Biol.* 2004;24:2284–2289.
5. Hutter R, Carrick FE, Valdiviezo C, Wolinsky C, Rudge JS, Wiegand SJ, Fuster V, Badimon JJ, Sauter BV. Vascular endothelial growth factor regulates reendothelialization and neointima formation in a mouse model of arterial injury. *Circulation.* 2004;110:2430–2435.
6. Bhardwaj S, Roy H, Heikura T, Yla-Herttuala S. VEGF-A, VEGF-D and VEGF-D(DeltaNDeltaC) induced intimal hyperplasia in carotid arteries. *Eur J Clin Invest.* 2005:669–676.
7. Hedman M, Hartikainen J, Syvanne M, Stjernvall J, Hedman A, Kivela A, Vanninen E, Mussalo H, Kauppila E, Simula S, Narvanen O, Rantala A, Peuhkurinen K, Nieminen MS, Laakso M, Yla-Herttuala S. Safety and feasibility of catheter-based local intracoronary vascular endothelial growth factor gene transfer in the prevention of postangioplasty and in-stent restenosis and in the treatment of chronic myocardial ischemia: phase II results of the Kuopio Angiogenesis Trial (KAT). *Circulation.* 2003;107:2677–2683.
8. Laitinen M, Hartikainen J, Hiltunen MO, Eranen J, Kiviniemi M, Narvanen O, Makinen K, Manninen H, Syvanne M, Martin JF, Laakso M, Yla-Herttuala S. Catheter-mediated vascular endothelial growth factor gene transfer to human coronary arteries after angioplasty. *Hum Gene Ther.* 2000;11:263–270.
9. Shiojima I, Walsh K. The role of vascular endothelial growth factor in restenosis: the controversy continues. *Circulation.* 2004;110:2283–2286.
10. Kendall RL, Wang G, Thomas KA. Identification of a natural soluble form of the vascular endothelial growth factor receptor, FLT-1, and its heterodimerization with KDR. *Biochem Biophys Res Commun.* 1996;226:324–328.
11. Millauer B, Wizigmann-Voos S, Schnurch H, Martinez R, Moller NP, Risau W, Ullrich A. High affinity VEGF binding and developmental expression suggest Flk-1 as a major regulator of vasculogenesis and angiogenesis. *Cell.* 1993;72:835–846.
12. Bussolati B, Dunk C, Grohman M, Kontos CD, Mason J, Ahmed A. Vascular endothelial growth factor receptor-1 modulates vascular endothelial growth factor-mediated angiogenesis via nitric oxide. *Am J Pathol.* 2001;159:993–1008.
13. Barleon B, Sozzani S, Zhou D, Weich HA, Mantovani A, Marme D. Migration of human monocytes in response to vascular endothelial growth factor (VEGF) is mediated via the VEGF receptor flt-1. *Blood.* 1996;87:3336–3343.
14. Hiratsuka S, Minowa O, Kuno J, Noda T, Shibuya M. Flt-1 lacking the tyrosine kinase domain is sufficient for normal development and angiogenesis in mice. *Proc Natl Acad Sci U S A.* 1998;95:9349–9354.
15. Zhao Q, Ishibashi M, Hiasa K, Tan C, Takeshita A, Egashira K. Essential role of vascular endothelial growth factor in angiotensin II-induced vascular inflammation and remodeling. *Hypertension.* 2004;44:264–270.
16. Kondo K, Hiratsuka S, Subbalakshmi E, Matsushime H, Shibuya M. Genomic organization of the flt-1 gene encoding for vascular endothelial growth factor (VEGF) receptor-1 suggests an intimate evolutionary relationship between the 7-Ig and the 5-Ig tyrosine kinase receptors. *Gene.* 1998;208:297–305.
17. Sata M, Maejima Y, Adachi F, Fukino K, Saiura A, Sugiura S, Aoyagi T, Imai Y, Kurihara H, Kimura K, Omata M, Makuuchi M, Hirata Y, Nagai R. A mouse model of vascular injury that induces rapid onset of medial cell apoptosis followed by reproducible neointimal hyperplasia. *J Mol Cell Cardiol.* 2000;32:2097–2104.
18. Masuda T, Ohmi K, Yamaguchi H, Hasegawa K, Sugiyama T, Matsuda Y, Iino M, Nonomura Y. Growing and differentiating characterization of aortic smooth muscle cell line, p53LMAC01 obtained from p53 knock out mice. *Mol Cell Biochem.* 1999;190:99–104.

19. Egashira K. Molecular mechanisms mediating inflammation in vascular disease: special reference to monocyte chemoattractant protein-1. *Hypertension*. 2003;41:834–841.
20. Egashira K, Nakano K, Ohtani K, Funakoshi K, Zhao G, Ihara Y, Koga J, Kimura S, Tominaga R, Sunagawa K. Local delivery of anti-monocyte chemoattractant protein-1 by gene-eluting stents attenuates in-stent stenosis in rabbits and monkeys. *Arterioscler Thromb Vasc Biol*. 2007;27: 2563–2568.
21. Inoue S, Egashira K, Ni W, Kitamoto S, Usui M, Otani K, Ishibashi M, Hiasa K, Nishida K, Takeshita A. Anti-monocyte chemoattractant protein-1 gene therapy limits progression and destabilization of established atherosclerosis in apolipoprotein E-knockout mice. *Circulation*. 2002;106:2700–2706.
22. Nakano K, Egashira K, Ohtani K, Zhao G, Funakoshi K, Ihara Y, Sunagawa K. Catheter-based adenovirus-mediated anti-monocyte chemoattractant gene therapy attenuates in-stent neointima formation in cynomolgus monkeys. *Atherosclerosis*. 2007;194:309–316.
23. Marumo T, Schini-Kerth VB, Fisslthaler B, Busse R. Platelet-derived growth factor-stimulated superoxide anion production modulates activation of transcription factor NF-kappaB and expression of monocyte chemoattractant protein 1 in human aortic smooth muscle cells. *Circulation*. 1997;96:2361–2367.
24. Egashira K, Zhao Q, Kataoka C, Ohtani K, Usui M, Charo IF, Nishida K, Inoue S, Katoh M, Ichiki T, Takeshita A. Importance of monocyte chemoattractant protein-1 pathway in neointimal hyperplasia after periarterial injury in mice and monkeys. *Circ Res*. 2002;90:1167–1172.
25. Ohtani K, Usui M, Nakano K, Kohjimoto Y, Kitajima S, Hirouchi Y, Li XH, Kitamoto S, Takeshita A, Egashira K. Antimonocyte chemoattractant protein-1 gene therapy reduces experimental in-stent restenosis in hypercholesterolemic rabbits and monkeys. *Gene Ther*. 2004;11: 1273–1282.
26. Usui M, Egashira K, Ohtani K, Kataoka C, Ishibashi M, Hiasa K, Katoh M, Zhao Q, Kitamoto S, Takeshita A. Anti-monocyte chemoattractant protein-1 gene therapy inhibits restenotic changes (neointimal hyperplasia) after balloon injury in rats and monkeys. *Faseb J*. 2002;16: 1838–1840.
27. Yamada M, Kim S, Egashira K, Takeya M, Ikeda T, Mimura O, Iwao H. Molecular mechanism and role of endothelial monocyte chemoattractant protein-1 induction by vascular endothelial growth factor. *Arterioscler Thromb Vasc Biol*. 2003;23:1996–2001.
28. Parenti A, Bellik L, Brogelli L, Filippi S, Ledda F. Endogenous VEGF-A is responsible for mitogenic effects of MCP-1 on vascular smooth muscle cells. *Am J Physiol Heart Circ Physiol*. 2004;286:H1978–H1984.
29. Griendling KK, FitzGerald GA. Oxidative stress and cardiovascular injury: Part I: basic mechanisms and in vivo monitoring of ROS. *Circulation*. 2003;108:1912–1916.
30. Viedt C, Vogel J, Athanasiou T, Shen W, Orth SR, Kubler W, Kreuzer J. Monocyte chemoattractant protein-1 induces proliferation and interleukin-6 production in human smooth muscle cells by differential activation of nuclear factor-kappaB and activator protein-1. *Arterioscler Thromb Vasc Biol*. 2002;22:914–920.
31. Ishida A, Murray J, Saito Y, Kanthou C, Benzakour O, Shibuya M, Wijelath ES. Expression of vascular endothelial growth factor receptors in smooth muscle cells. *J Cell Physiol*. 2001;188:359–368.
32. Khurana R, Zhuang Z, Bhardwaj S, Murakami M, De Muinck E, Yla-Herttuala S, Ferrara N, Martin JF, Zachary I, Simons M. Angiogenesis-dependent and independent phases of intimal hyperplasia. *Circulation*. 2004;110:2436–2443.
33. Asahara T, Bauters C, Pastore C, Kearney M, Rossow S, Bunting S, Ferrara N, Symes JF, Isner JM. Local delivery of vascular endothelial growth factor accelerates reendothelialization and attenuates intimal hyperplasia in balloon-injured rat carotid artery. *Circulation*. 1995;91: 2793–2801.

Supplemental Figure I

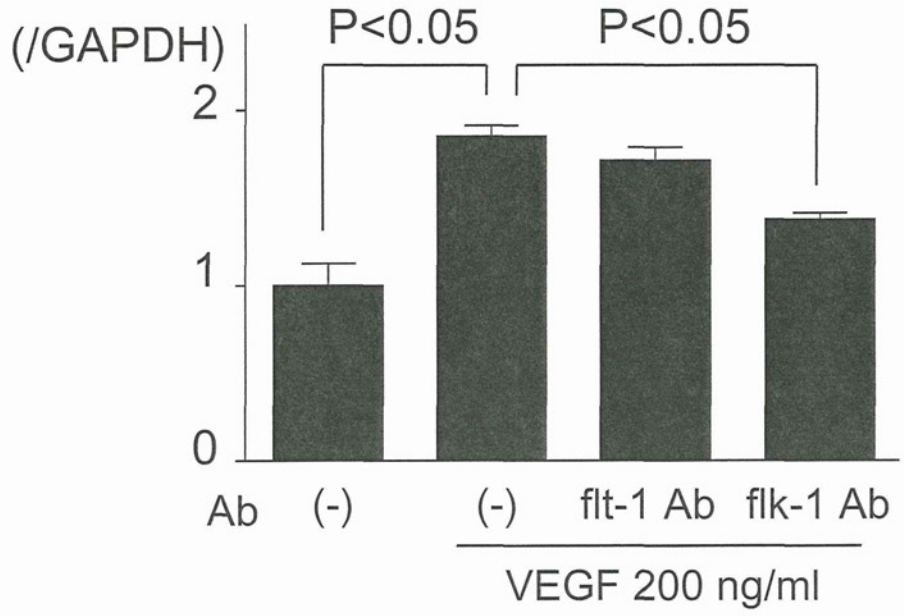

Supplemental Figure II

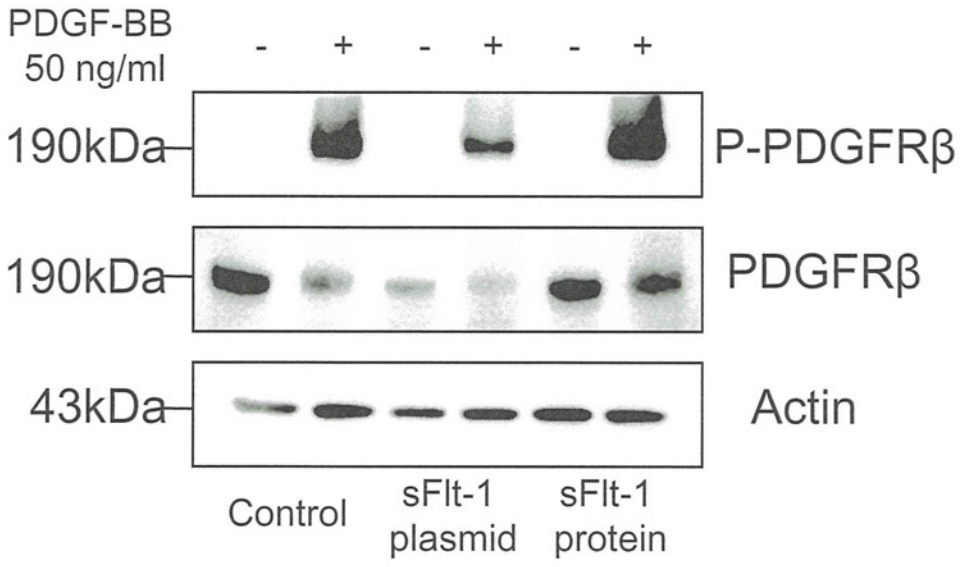

Circ J 2009; **73:** 381–383

Intracardiac Echocardiography-Guided Cardiac Tumor Biopsy

Taiki Higo, MD; Masao Takemoto, MD; Kiyohiro Ogawa, MD; Shujiro Inoue, MD; Ken-ichi Eshima, MD; Hideo Tada, MD; Kenji Sunagawa, MD

A 63-year-old woman was admitted to hospital with the chief complaint of new onset chest discomfort and pretibial pitting edema. Transthoracic echocardiography revealed a large invasive tumor on the heart protruding into the right atrium and right ventricle, which obstructed the outflow tract. She underwent transvenous 9Fr, 9-MHz ultra intracardiac echocardiography (ICE) (EP Technologies, Boston Scientific Corporation, San Jose, CA, USA) guided biopsy, and a diagnosis of malignant lymphoma was established from the specimen obtained. ICE-guided cardiac tumor biopsy may be one of the most useful strategies for diagnosis of cardiac tumors. (*Circ J* 2009; **73:** 381–383)

Key Words: Biopsy; Cardiac tumor; Diagnosis; Intracardiac echocardiography; Malignant lymphoma

Although primary cardiac tumors are relatively rare,[1] physicians unexpectedly encounter them in clinical practice and it is important to establish a histopathological diagnosis in order to treat them adequately; however, it is difficult to do so non-invasively. We describe a case of a primary cardiac malignant lymphoma that was easily and safely diagnosed histopathologically after a transvenous intracardiac echocardiography (ICE)-guided biopsy.

Case Report

A 63-year-old woman was admitted to hospital with the chief complaint of new onset chest discomfort and pretibial pitting edema. On physical examination, dilated jugular veins and pretibial pitting edema were noted. Auscultation revealed a cardiac ejection systolic murmur and normal vesicular lung sounds. Chest X-ray revealed cardiomegaly (cardiothoracic ratio=64%), and the electrocardiogram demonstrated right-axis deviation, right bundle blanch block, low voltage in the limb leads, and poor R wave progression in the precordial leads. Transthoracic echocardiography (TTE) revealed a large invasive cardiac tumor protruding into the right atrium (RA) and right ventricle (RV), obstructing the outflow tract (RVOT) (**Figs 1A,B**). There was also moderate pericardial effusion without any hemodynamic significance. Contrast computed tomography (CT) also showed the large cardiac tumor measuring 76×37 mm in diameter and stretching from the RA to the RV and pulmonary artery (**Fig 2**). Pericardial effusion, as

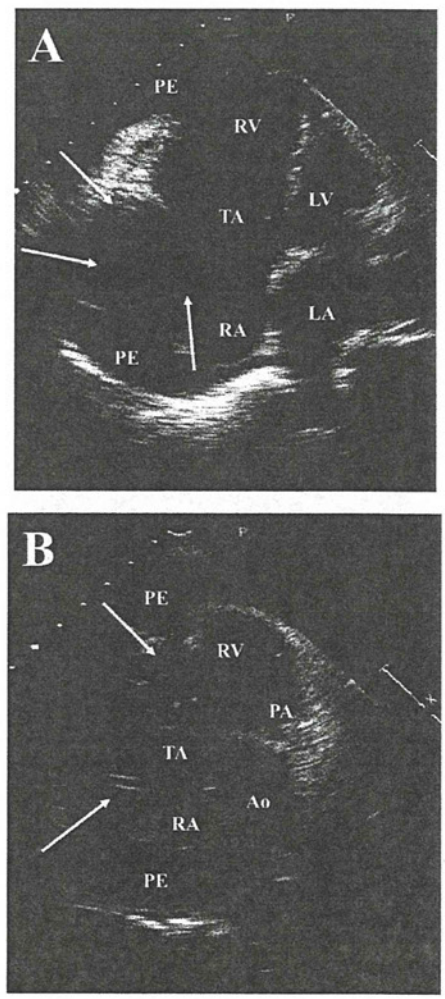

Fig 1. Two-dimensional transthoracic echocardiograms on admission in the apical 4-chamber view (**A**) and short-axis view (**B**) show the large invasive cardiac tumor (white arrows) protruding into the right atrium (RA) and right ventricle (RV), and causing an RV outflow tract obstruction. PA, pulmonary artery; PE, pericardial effusion; TA, tricuspid valve annulus; LA, left atrium; LV, left ventricle; Ao, aorta.

(Received January 15, 2008; revised manuscript received March 5, 2008; accepted April 29, 2008; released online December 5, 2008)
Department of Cardiovascular Medicine, Kyushu University Hospital, Fukuoka, Japan
There is no conflict of interest related to this study.
Mailing address: Masao Takemoto, MD, Department of Cardiovascular Medicine, Kyushu University Hospital, 3-1-1 Maidashi, Higashi-ku, Fukuoka 812-8582, Japan. E-mail: matakemo@cardiol.med.kyushu-u.ac.jp

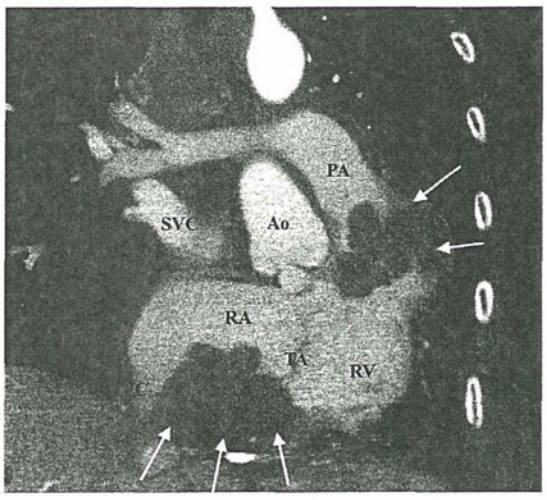

Fig 2. Contrast computed tomographic image shows the cardiac tumor (white arrows) protruding into the right atrium (RA) and right ventricle (RV), and causing an RV outflow tract obstruction. Ao, aorta; PA, pulmonary artery; TA, tricuspid valve annulus; SVC, superior vena cava; IVC, inferior vena cava.

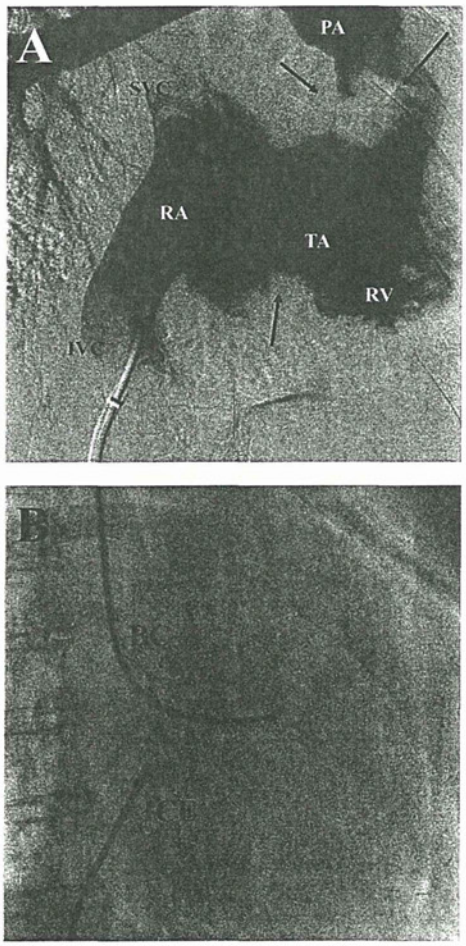

Fig 3. Right anterior oblique (RAO) view of a right atriogram (**A**) showing the cardiac tumor (black arrows) protruding into the right atrium (RA) and right ventricle (RV), and causing an RV outflow tract obstruction. RAO view of a fluoroscopic image (**B**) shows the location of the biopsy catheter (BC) next to the cardiac tumor and the intracardiac echocardiography (ICE) catheter in the RA. PA, pulmonary artery; TA, tricuspid valve annulus; SVC, superior vena cava; IVC, inferior vena cava.

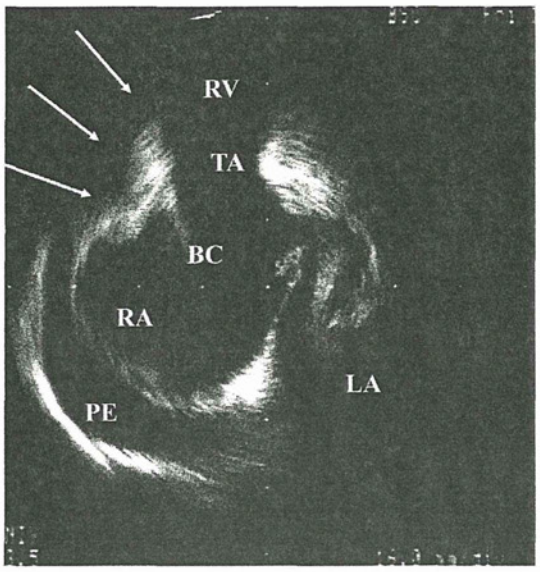

Fig 4. Intracardiac echocardiographic image shows the biopsy catheter (BC) next to the cardiac tumor (white arrows) protruding into the right atrium (RA) and right ventricle (RV). PE, pericardial effusion; TA, tricuspid valve annulus; LA, left atrium.

well as mediastinal and mesenteric lymphadenopathy, were revealed. Because the cytology examination from the pericardial effusion was negative, a percutaneous cardiac tumor biopsy was performed in order to establish a histopathological diagnosis. Right atriography also revealed the cardiac tumor protruding into the RA and RV (**Fig 3A**). A 6Fr cardiac biopsy catheter (Technowood Biopsy Forceps, Tonokura Ika Kogyo Co Ltd, Tokyo, Japan) and 9Fr, 9-MHz Ultra ICE catheter (EP Technologies, Boston Scientific Corporation, San Jose, CA, USA) were percutaneously inserted into the RA via the right jugular vein and right femoral vein, respectively (**Fig 3B**). Because ICE images enabled detailed examination of the intracardiac structures, as well as an accurate surveillance of the positioning of the biopsy catheter (**Fig 4**), cardiac tumor specimens were easily and safely taken without any complications, pain, or exposure of the echocardiographer to radiation. Histopathological analysis showed diffuse large B-cell lymphoma. The patient underwent R-THPCOP chemotherapy (rituximab, pirarubicin, cyclosporin, vincristine, and prednisolone). During the first month following the treatment, her condition improved, which correlated with the finding of a decrease in the tumor size, and resolution of the pericardial effusion and RVOT obstruction on TTE. She has remained well under chemotherapy as an outpatient.

Discussion

Primary cardiac tumors are relatively rare with an incidence of 0.002–0.3% in autopsy series;[1] however, physicians unexpectedly encounter them in clinical practice and although the exact incidence of each specific tumor type can not be stated, approximately 75% of all cardiac tumors are histologically benign and the remainder are malignant.[2] Sarcomas are the most common malignant primary cardiac tumors and primary cardiac lymphomas are much less common,[3] with a relative incidence of only 2% of primary cardiac tumors.

The available and useful noninvasive diagnostic tools

such as echocardiography, CT, and magnetic resonance imaging can provide much important information regarding the size, shape, composition, attachment, and surface characteristics of tumors[4,5] which are important considerations for surgical excision, but surgery is not an effective treatment for the great majority of malignant cardiac tumors, because of the large mass of cardiac tissue involved, as in the present case, and because all cardiac tumors have the potential for causing life-threatening complications[6] including embolization. Thus, it is critically important to establish a histopathlogical diagnosis for instigation of appropriate treatment as soon as possible.

Previous reports demonstrate that a transvenous biopsy under TTE or transesophageal echocardiographic (TEE) guidance[4,7,8] is a useful diagnostic approach. Although TTE is the most noninvasive and convenient technique, TEE can provide superior imaging to TTE, especially of posteriorly located structures[9] However, TEE sometimes causes the patient pain if performed without anesthesia, and for that reason it may usually requires local pharyngeal anesthesia and sometimes general sedation. Moreover, the operator of the TTE or TEE is at risk of exposure to radiation during the procedure.

ICE is a new technique based on the use of an ultrasonic diagnostic catheter that can be introduced through the femoral vein and provides a 2-dimensional view[10] Image acquisition is usually from within the RA or RV. Thus, ICE enables complete examination of the inter-atrial and -ventricular structures, as well as an accurate surveillance of the positioning of intracardiac devices[11] such as a biopsy catheter. A major advantage of ICE is its potential to provide superior information to TEE;[10,11] as well as avoiding general sedation and exposure of the echocardiographer to radiation. Therefore, ICE may be one of the most useful diagnostic strategies and should be considered when trying to diagnose the histopathology of cardiac tumors. At present, however, the main limiting factor is its high cost, which is related to the single-use catheters.

Acknowledgments

We thank Kazutaka Yamaguchi for his technical assistance for intracardiac echocardiography, and John Martin for his linguistic assistance with this paper.

References

1. Reynen K. Frequency of primary tumors of the heart. *Am J Cardiol* 1996; **77:** 107.
2. Lam KY, Dickens P, Chan AC. Tumors of the heart: A 20-year experience with a review of 12,485 consecutive autopsies. *Arch Pathol Lab Med* 1993; **117:** 1027–1031.
3. Kasai K, Kuwao S, Sato Y, Murayama M, Harano Y, Kameya T. Case report of primary cardiac lymphoma: The applications of PCR to the diagnosis of primary cardiac lymphoma. *Acta Pathol Jpn* 1992; **42:** 667–671.
4. Abramowitz Y, Hiller N, Perlman G, Admon D, Beeri R, Chajek-Shaul T, et al. The diagnosis of primary cardiac lymphoma by right heart catheterization and biopsy using fluoroscopic and transthoracic echocardiographic guidance. *Int J Cardiol* 2007; **118:** e39–e40.
5. Sato Y, Matsumoto N, Kinukawa N, Matsuo S, Komatsu S, Kunimasa T, et al. Successful treatment of primary cardiac B-cell lymphoma: Depiction at multislice computed tomography and magnetic resonance imaging. *Int J Cardiol* 2006; **113:** E26–E29.
6. Harvey WP. Clinical aspects of cardiac tumors. *Am J Cardiol* 1968; **21:** 28–43.
7. Kang SM, Rim SJ, Chang HJ, Choi D, Cho SY, Cho SH, et al. Primary cardiac lymphoma diagnosed by transvenous biopsy under transesophageal echocardiographic guidance and treated with systemic chemotherapy. *Echocardiography* 2003; **20:** 101–103.
8. Jurkovich D, de Marchena E, Bilsker M, Fierro-Renoy C, Temple D, Garcia H. Primary cardiac lymphoma diagnosed by percutaneous intracardiac biopsy with combined fluoroscopic and transesophageal echocardiographic imaging. *Catheter Cardiovasc Interv* 2000; **50:** 226–233.
9. Edwards LC 3rd, Louie EK. Transthoracic and transesophageal echocardiography for the evaluation of cardiac tumors, thrombi, and valvular vegetations. *Am J Card Imaging* 1994; **8:** 45–58.
10. Girod G, Delabays A, Roguelov C, Renders F, Van de Walle S, Vogt P, et al. Intracardiac echocardiography: A new tool for interventional cardiology. *Rev Med Suisse* 2007; **3:** 1696–1701.
11. Brochet E, Habib G. Intracardiac echocardiography during percutaneous closure of atrial septal defect and patent foramen ovale. *Arch Mal Coeur Vaiss* 2005; **98:** 25–28.

Free Radical Research, January 2009; 43(1): 37–46

informa
healthcare

Time-dependent changes of myocardial and systemic oxidative stress are dissociated after myocardial infarction

TAKAHIRO INOUE[1], TOMOMI IDE[1], MAYUMI YAMATO[2], MASAYOSHI YOSHIDA[1], TAKAKI TSUTSUMI[1], MAKOTO ANDOU[1], HIDEO UTSUMI[3], HIROYUKI TSUTSUI[4], & KENJI SUNAGAWA[1]

[1]*Department of Cardiovascular Medicine, Graduate School of Medical Sciences,* [2]*Department of REDOX Medicinal Science,* [3]*Department of Bio-functional Science, Graduate School of Pharmaceutical Sciences, Kyushu University, Fukuoka 812-8582, Japan, and* [4]*Department of Cardiovascular Medicine, Hokkaido University Graduate School of Medicine, Sapporo 060-8638, Japan*

Accepted by Professor G. Mann

(Received 10 July 2008; revised 17 September 2008)

Abstract
Reactive oxygen species (ROS) is increased in myocardium after myocardial infarction (MI), which may play a causal role in cardiac remodelling. However, there is scant direct and longitudinal evidence that systemic oxidative stress is enhanced accompanying an increase of ROS in myocardium. The authors conducted a comprehensive investigation of ROS markers by simultaneously sampling urine, blood and myocardium and *in vivo* ESR for the heart at different stages of post-MI cardiac remodelling in mouse with permanent occlusion of left coronary artery. Systemic oxidative markers increased at early days after MI and were normalized later. In contrast, TBARS and 4-hexanoyl-Lys staining were increased in non-infarct myocardium at day 28. The enhancement of ESR signal decay of methoxycarbonyl-PROXYL measured at the chest was associated with the progression of left ventricle dilatation and dysfunction. This study provided the direct evidence that redox alteration and production of ROS occurred in myocardium during the progression of cardiac remodelling and failure; however, ROS marker levels in blood and urine do not reflect the production of ROS from failing myocardium.

Keywords: *Myocardial remodelling, oxidative stress markers, heart failure, in vivo ESR*

Abbreviations: *LV, left ventricular; MI, myocardial infarction; HF, heart failure; RAS, renin-angiotensin system; ROS, reactive oxygen species; MMP, matrix metalloproteinase; TBARS, thiobarbituric acid reactive substances; 8-OH-dG, 8-hydroxy-2′-deoxyguanosine; GPx, glutathione peroxidase; SOD, superoxide dismutase; HEL, Nε-(Hexanoyl) Lysin; ESR, electron spin resonance; FS, fractional shortening; HR, heart rate; LVEDD, left ventricular end-diastolic dimension; LVESD, left ventricular end-systolic dimension; 3-methoxycarbonyl-PROXYL, 3-methoxycarbonyl-2,2,5,5-tetramethylpyrrolidine-1-oxyl*

Introduction

Pathological left ventricular (LV) remodelling after myocardial infarction (MI) is increasingly recognized as the major cause of heart failure (HF) [1]. MI induces alterations of LV architecture with scar formation, ventricular dilatation and hypertrophy of the non-infarct myocardium [2]. In the process of remodelling, activation of various neurohumoral factors and inflammatory response, including activation of the

Correspondence: Tomomi Ide, MD, PhD, Department of Cardiovascular Medicine, Kyushu University Graduate School of Medicine, 3-1-1, Maidashi, Higashi-ku, Fukuoka 812-8582, Japan. Tel: +81-92-642-5360. Fax: +81-92-642-5374. Email: tomomi_i@cardiol.med.kyushu-u.ac.jp

ISSN 1071-5762 print/ISSN 1029-2470 online
DOI: 10.1080/10715760802534820

renin-angiotensin system (RAS), contributes to healing and scar formation in the infarct myocardium. At the end of the repairing process, cardiac hypertrophy due to haemodynamic overload is associated with hypertrophic growth of cardiomyocytes accompanying fibrosis and inappropriate interstitial collagen formation. The prognosis of HF remains poor even with wide use of RAS inhibitors and β adrenergic receptor blockers [3]. Recently, growing evidence has suggested that reactive oxygen species (ROS) are involved in the pathophysiology of myocardial remodelling and failure [4–10] and increases of ROS have been shown in various animal models of HF. We and others have demonstrated that generation of ROS is increased in post-MI myocardium in mice [9] and that treatment with antioxidants or over-expression of antioxidant enzymes prevents cardiac remodelling [11–13], resulting in improvement of survival after MI [12,13]. *In vitro* experiments demonstrated that ROS mediate hypertrophy in cardiomyocytes induced by neurohumoral factors such as angiotensin II and catecholamines, as well as cytokines including TNFα [14–17]. ROS modulate extracellular matrix function via their effects on fibroblast proliferation and collagen synthesis, involving redox-sensitive activation of matrix metalloproteinases (MMPs) [11,18,19]. Moreover, ROS alter gene expression in the case of intracellular Ca^{2+} overload, activating various proteases and promoting apoptosis in cardiomyocytes [20,21]. The above findings thus strongly suggest that redox regulation may be a potential therapeutic strategy for cardiac remodelling and HF. However, despite much discussion on the biological activities of ROS in remodelling, there is scanty clinical or animal experimental evidence for elevation of systemic oxidative biomarkers corresponding to the increase of ROS in the remodelling myocardium. We thus examined the time courses of oxidative stress in the post-MI myocardium and in systemic circulation by performing simultaneous sampling of urine, blood and myocardium during the post-MI course in a HF mouse model. Since the effects of ROS depend on a balance between the pro-oxidant molecules generated and the antioxidant reserve *in vivo*, both components should be tested to obtain better understanding of the effects of ROS on the progression of remodelling. For a comprehensive investigation of oxidative stress, we measured the byproducts of ROS represented by thiobarbituric acid reactive substances (TBARS) and 8-hydroxy-2′-deoxyguanosine (8-OH-dG), as well as the antioxidant defense capacity indicated by scavenger enzymes. Moreover, excised biological specimens only enable one to identify the target of ROS after the exposure to ROS but not to reflect the dynamic changes of redox status *in vivo* in the chronic HF model. Accordingly, we applied *in vivo* ESR to estimate redox status non-invasively in the process of remodelling using a post-MI HF model in mice.

Materials and methods

Animal model

This experiment conformed with the Guide for the Care and Use of Laboratory Animals published by the US National Institute of Health and was reviewed and approved by the Committee of the Ethics on Animal Experiment, Kyushu University Graduate School of Medical Sciences, and performed in compliance with the relevant Law (No. 105) and Notification (No. 6) of the Japanese Government.

Six week-old CD-1 male mice were purchased from Kyudo Co., Ltd. (Saga, Japan). The mice were housed in a temperature- and humidity-controlled room. MI was experimentally induced in mice by ligating the left coronary artery permanently, as previously reported [11]. The mice were assigned randomly into five groups; post-MI days 1, 4, 7, 14 and 28, and the survived mice (survived/operated: $n = 6/7$, 6/8, 10/14, 9/11, 14/21, respectively) were used in the experiments on the assigned days. Urine, blood and myocardium samples were collected from each mouse. The myocardial samples of all six mice on post-MI day 4 and six mice on post-MI day 28 were examined immunohistochemically, while the samples of the other mice were used for biochemical analysis. The data were compared with those from control mice that underwent sham operation without coronary artery ligation at day 28 ($n = 7$).

Echocardiography and haemodynamic measurements

Echocardiographic studies were performed under light anaesthesia by an intraperitoneal injection of sodium pentobarbital, with spontaneous respiration before the animal was euthanized. A 2D parasternal short-axis view of the LV was obtained by applying the transducer lightly to the mid-upper left anterior chest wall. The transducer was then gently moved cephalad or caudad and angulated until desirable images were obtained. After ensuring that the image was on axis (based on roundness of the LV cavity), 2D targeted M-mode tracings were recorded at a paper speed of 50 mm/s. Our previous study showed small intra-observer and inter-observer variabilities of our echocardiographic measurements for LV dimensions and high reproducibility of measurements made in the same animals on separate days [22]. Under the same anaesthesia with Avertin, a 1.4 Fr micromanometer-tipped catheter (Millar Instruments) was inserted into the right carotid artery and then advanced into the LV for the measurement of LV pressures for the assessment of severity of HF at day 28 after MI.

Blood sampling

Blood sample was collected with 1:500 dilution of heparin just before euthanizing each animal. Plasma was separated by centrifugation at $1000 \times g$ for 15 min at 4°C and stored at −80°C until analysis. The erythrocyte fraction was washed three times with isotonic NaCl. A stock haemolysate was prepared by the addition of the 2-mercaptoethanol-EDTA stabilizing solution. The concentrated haemolysate was diluted with 2% ethanol immediately before assay.

TBARS in plasma and 8-OH-dG in urine

To assess the level of systemic oxidative stress generated in the process of cardiac remodelling after MI, we measured TBARS in plasma and 8-OH-dG in urine. Plasma TBARS was measured by fluorometric analysis. The plasma was pre-treated with 10% phosphotungstic acid and 1/12 N sulphuric acid. The sample was mixed with a reagent to obtain a final concentration of 7.5% acetic acid, 2 mmol/L EDTA and 0.4% SDS and then reacted with 0.3% thiobarbituric acid (TBA) in a boiling water bath for 45 min. After cooling, the chromogen was extracted in n-butanol/pyridine (15:1, v/v). Fluorescence of the supernatant was measured at excitation and emission wavelengths of 510 and 550 nm, respectively, using a GENios Pro™ (Tecan Group Ltd. Durham, NC). The standard was prepared using 1,1,3,3, -tetraethoxypropane (TEP).

Urine samples were collected in individual metabolic cages (Nalgen, Rochester, NY). After overnight fasting, urine sample was collected from each mouse. Urine 8-OH-dG concentration was determined using a competitive ELISA kit (8-OH-dG check®, Japan, Institute for the Control of Aging, Nagoya, Japan). The value was corrected by urinary creatinine measured with a colorimetric assay kit (Sigma, St. Louis, MO).

TBARS in myocardial tissue

The myocardium was homogenized in 10 volumes of 50 mmol/L sodium phosphate buffer at 4°C for the assay of TBARS in myocardium. The homogenate was centrifuged at $4500 \times g$ for 15 min and the supernatant was used for the biochemical assay of TBARS as in plasma.

Antioxidant enzyme activities in myocardium

To determine the change in capacity of defense during the progression of cardiac remodelling, we measured the levels of antioxidant enzyme activities in the myocardium.

The enzymatic activities of glutathione peroxidase (GPx) and superoxide dismutase (SOD) were measured spectrophotometrically (Tecan Group Ltd., GENios). GPx activity was determined according to the method of Yamamoto and Takahashi [23] by following the oxidation of NADPH in the presence of GR (Oriental Yeast Co., Ltd. Tokyo, Japan), which catalyses the reduction of oxidized glutathione (GSSH) formed by GPx. One enzyme unit is defined as the amount of enzyme that oxidizes 1 μmol of NADPH per minute. SOD activity was examined by the cytochrome c method, in which xanthine and xanthine oxidase (Oriental Yeast Co., Ltd. Tokyo, Japan) were used as a source of superoxide. A unit was defined as the quantity of SOD required for 50% inhibition of the rate of cytochrome c reduction (Wako Pure Chemical Industries, Inc. Osaka, Japan). Protein concentration was determined by the Bradford assay.

Hexanoyl-Lysine adduct (HEL) immunostaining in myocardial tissue

Left ventricular myocardial sections obtained from mice at baseline, day 3 and 28 after MI were immunolabelled by a specific monoclonal anti-HEL antibody (Nikkenn SEIL Corp.). Paraffin-embedded tissue sections (5-μm thick) were deparaffinized with xylene, refixed in Bouin's solution for 20 min, immersed in PBS, incubated with 0.3% H_2O_2 in methanol for 30 min, followed by blocking with M.O.M. mouse IgG blocking reagent. The sections were further incubated with monoclonal anti-HEL antibody in M.O.M. Diluent. After rinsing with 10 mmol/L PBS, they were incubated with biotin-labelled goat anti-rabbit IgG anti-serum (1:100 dilution; DAKO A/S) for 60 min and then with avidin-biotin complex (1:100 dilution; Vectastain ABC kit) for 60 min. After rinsing, the sections were finally incubated with 0.02% 3,3-diaminobenzidine and 0.03% H_2O_2 in deionized water for 6–9 min. As a negative control, sections were incubated with normal rabbit serum instead of anti-HEL antibody.

In vivo *electron spin resonance study*

A spin probe, 3-methoxycarbonyl-2,2,5,5-tetramethylpyrrolidine-1-oxyl (methoxycarbonyl-PROXYL) was synthesized as described previously [24]. For the *in vivo* ESR measurements, 100 mmol/L isotonic methoxycarbonyl-PROXYL was administered (3 μl/g body weight) in mice intravenously. Then ESR spectra were taken at regular intervals using a L-band ESR spectrometer (JEOL Co. Ltd., Akishima, Japan) with a loop-gap resonator (33 mm i.d. and 30 mm in length), as reported previously [25,26]. The power of the 1.1 GHz microwave was 10 mW. The amplitude of the 100-kHz field modulation was 0.063 mT. The signal decay rates, which were used as an index of ROS generation, were determined from the semi-logarithmic plots of signal

intensity vs time after probe injection. Tiron or dimethylthiourea (DMTU) (3 μmol/mouse, dissolved in saline) was administered simultaneously with the probe to confirm the relationship between the signal decay and ROS generation.

Statistical analysis

All data are expressed as mean ± SEM. Between-group comparisons of the means were performed by one-way ANOVA followed by *t*-tests. Bonferroni's correction was done for multiple comparisons of means. A *p*-value less than 0.05 was considered to be statistically significant.

Results

Animal characteristics

The echocardiographic data of surviving mice at days 1, 4, 7, 14 and 28 after MI and control mice are shown in Table I. LV diameters were significantly greater in MI mice at day 4 and thereafter compared to sham-operated control mice. Moreover, MI mice had smaller fractional shortening and anterior wall thickness. There were no alterations in LV diameter and systolic function in sham-operated mice without coronary artery ligation up to day 28 after the operation (data not shown). At day 28, left ventricule LV end-diastolic pressure (LVEDP) was increased in MI (2.6 ± 0.7 vs 14.0 ± 2.3, $p < 0.01$) and LV weight (wt)/body wt (3.12 ± 0.11 vs 3.68 ± 0.17 mg/g, $p < 0.05$), RV wt/body wt (0.88 ± 0.06 vs 1.38 ± 0.11 mg/g, $p < 0.05$), lung wt/body wt (5.36 ± 0.13 vs 7.71 ± 0.80 mg/g, $p < 0.05$) were all increased in MI. The prevalence of pleural effusion was significantly higher in MI (0 vs 50%, $p < 0.01$).

Oxidative byproducts in plasma and urine

Plasma TBARS and urinary 8-OH-dG were significantly elevated at day 1 after MI (Figure 1), and declined to control levels at day 7 and thereafter.

Oxidative markers and antioxidant enzyme activity in myocardial tissue

We measured TBARS (an indicator of lipid peroxidation) and performed immunohistochemical staining of HEL in both infarct and non-infarct myocardial samples. In the infarct area, TBARS increased at day 1 and 7 after MI (Figure 2A). In the non-infarct area, on the contrary, TBARS level was not altered in the early days (days 1, 7 and 14) after MI but was elevated only at day 28.

In agreement with the results of myocardial TBARS, HEL-positive cardiomyocytes were located in the infarct area, whereas there was no staining in the non-infarct area at day 4. (Figure 3). HEL is a novel lipid hydroperoxide modified lysine residue, which is formed by oxidative modification by oxidized ω6 fatty acids such as linoleic acid or arachidonic acid. HEL is a useful biomarker for the initial stage of lipid peroxidation. Although positive staining lasted in the infarct area at day 28, the myocardium was mostly replaced by fibrous tissue and little living myocyte existed. In the non-infarct area, cardiomyocytes were hypertrophied and positively stained by HEL antibody. These suggest that lipid peroxidation starts at an early stage in the infarct area but at late remodelling stage in the non-infarct area. This is consistent with TBARS level in myocardium and indicated increased generation of ROS in the non-infarct area at day 28. The increase of TBARS in the non-infarct area was associated with a significant decline in SOD activity and a tendency of decrease in GPx activity at day 28 (Figure 4).

In vivo *ESR in the heart*

Since TBARS is known to be a non-specific assay to measure lipid peroxidation from biological fluids and tissues and many other substances besides reactive aldehydes react with TBA, we used *in vivo* ESR to determine whether the level of ROS increased in the heart in the remodelling process. Methoxycarbonyl-PROXYL, a stable membrane-permeable nitroxyl radical, is converted into its non-magnetic products, such as its hydroxylamine, immediately after the

Table I. Echocardiographic data.

		Time after MI (days)				
	Control	1	4	7	14	28
n	7	6	6	10	9	8
Heart rate (bpm)	524±22	564±25	552±16	568±23	551±28	589±43
LVEDD (mm)	4.0±0.2	4.5±0.2	5.0±0.2**	5.1±0.2**	5.4±0.1**	5.6±0.2**
LVESD (mm)	2.3±0.2	3.6±0.2**	3.9±0.2**	3.9±0.1**	4.2±0.1**	4.4±0.1**
Fractional shortening (%)	37.6±1.6	21.1±1.6**	22.2±1.6**	23.2±1.6**	20.7±1.0**	21.0±2.7**
Infarct wall thickness (mm)	0.83±0.03	0.60±0.05**	0.61±0.03**	0.44±0.02**	0.44±0.06**	0.30±0.08**
Non-infarct wall thickness (mm)	0.84±0.04	0.80±0.05	1.00±0.02	1.13±0.07*	1.30±0.05**	1.25±0.18**

Control, sham-operated mice; LV, left ventiruclar; EDD, end-diastolic dimension; ESD, end-systolic dimension.
Values are means ± SEM. * $p < 0.05$, ** $p < 0.01$ vs controls.

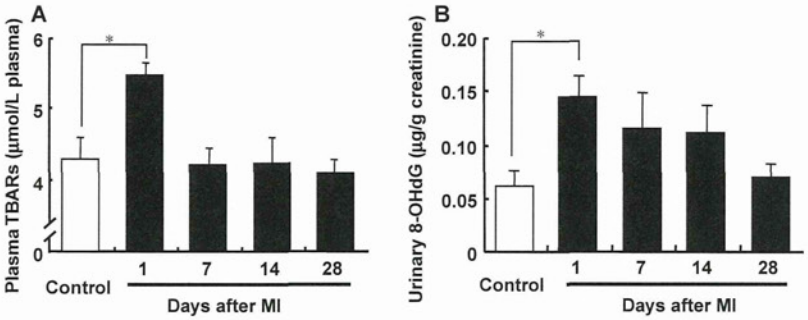

Figure 1. Time-dependent changes of plasma TBARs (A) and urinary 8-OHdG (B) in sham-operated control mice ($n=7$) and mice on day 1 ($n=6$), day 7 ($n=10$), day 14 ($n=9$) and day 28 ($n=8$) after MI. Values are means ± SEM. * $p<0.05$, ** $p<0.01$ compared with sham-operated control.

reaction with hydroxy radicals or other reductants. To determine the level of ROS or redox status by *in vivo* ESR measurements, we used methoxycarbonyl-PROXYL as a spin probe which was observed as three sharp lines by ESR spectroscopy (Figure 5A).

We applied signal decay of methoxycarbonyl-PROXYL to *in vivo* ESR to measure ROS generation non-invasively in the failing heart in mice after MI. When the ESR spectrum was measured at the chest level, the signal decay rate was greater in MI mice than sham-operated mice (Figure 5B). The increase of the signal decay observed in MI was suppressed by a simultaneous injection of antioxidants, Tiron or DMTU (Figure 5C and D), indicating the enhancement of free radical reactions at the chest in MI mice. To confirm that the enhancement of signal decay is localized at the chest and does not reflect the increase of systemic free radical generation, the same ESR measurement was repeated at the other parts of the body, head and abdomen from the same animals. ESR signal decay was similar between the two groups when the spectrum was detected at the head and abdominal levels (Figure 5E and F).

Redox alteration during the process of remodelling after MI

Using this *in vivo* ESR technique, we measured free radical production during the time course of remodelling after MI in mice. Radical generation was increased gradually in 4 weeks after MI, which was in parallel to the increase of LVEDD and LVESD and the decrease of EF assessed by echocardiography (Figure 6).

Discussion

In the post-MI myocardium, early remodelling occurs accompanied by infarct expansion, regional dilatation and thinning of the infarct zone and is followed by further deterioration in cardiac performance and increased neurohormonal activation in late remodelling. ROS play an important role in the progression of remodelling in the post-MI myocardium. However, phase-dependent alteration of ROS production in the post-MI myocardium has not been discussed. Moreover, despite a lack of evidence, it is widely misconstrued that an increase of local ROS production is reflected by increases of systemic ROS markers. The present study demonstrates that systemic elevations of ROS markers occur only at the earlier phase after MI. On the contrary, the generation of ROS in non-infarct myocardium is increased from the late phase.

Roles of ROS in the progression of cardiac remodelling

ROS potentially cause cellular damage and dysfunction. Whether the effects of ROS are beneficial or

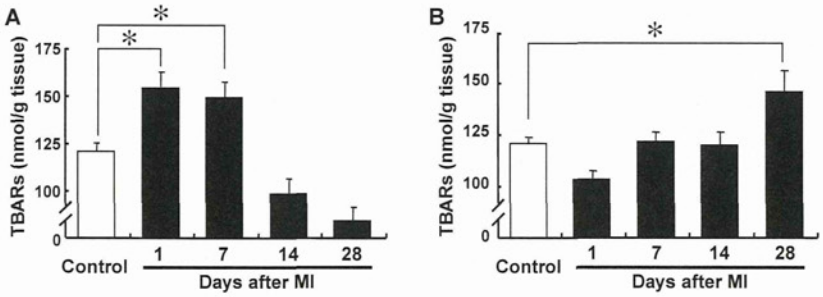

Figure 2. Time-dependent changes of TBARs in infarct (A) and in non-infarct (B) myocardium in sham-operated control ($n=7$) and on day 1 ($n=6$), day 7 ($n=10$), day 14 ($n=9$) and day 28 ($n=8$) after MI. Values are means ± SEM. * $p<0.05$ compared with sham-operated control.

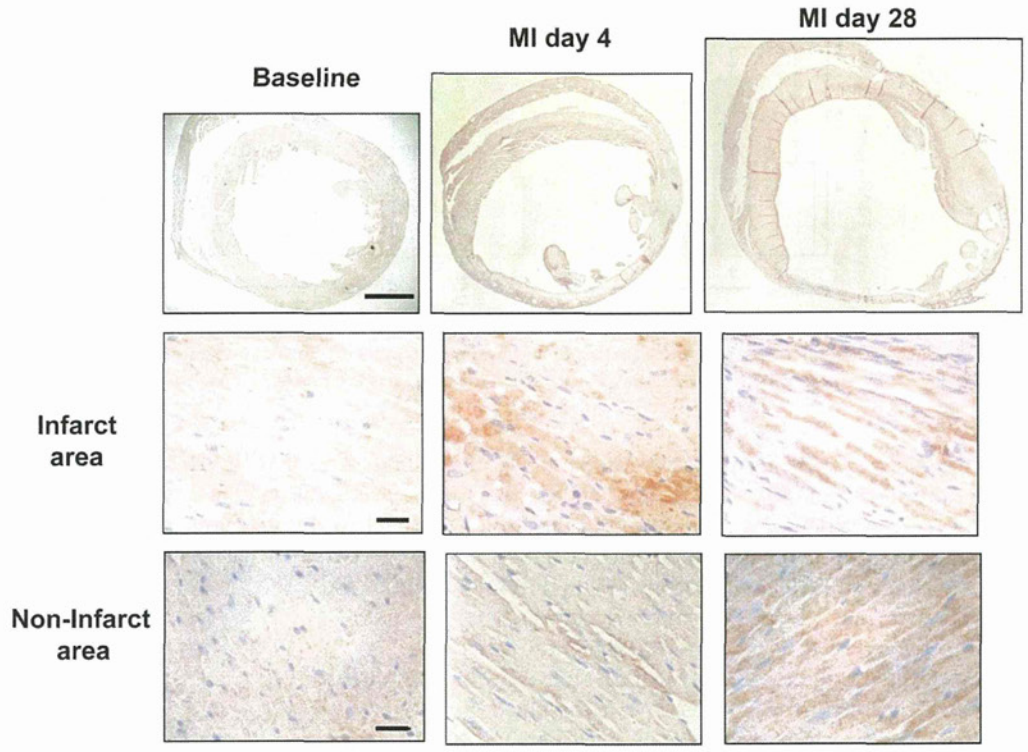

Figure 3. Immunohistochemical detection of HEL moieties in the remodelling process in whole LV, infarct myocardium and non-infarct myocardium, during acute-phase (day 4) and late-phase (day 28) after MI. Scale bar; 1 mm (top) and 10 μm (infarct area and non-infarct area).

harmful depends on the site of action, the source, the amount of ROS generation and the resulting redox balance. Several groups reported that ROS are increased in congestive HF patients [27,28] and accumulating evidence from animal studies revealed that increased ROS play a pivotal role in the pathogenesis and progression of HF [4,9,29–33]. However, whether systemic ROS markers are useful for determining the redox state of the failing heart remains unknown. Li et al. [34] used LC/MS/MS to analyse F_2-isoprostanes in urine from HF patients. They found that only a few peaks were increased, but the most abundant isomer 5-epi-8,12-iso-iP$F_{2\alpha}$-VI was comparable to control subjects. Other clinical studies examined ROS in serum or urine in HF patients by measuring redox markers and reported that ROS are elevated in functionally very poor, NYHA class III or class IV patients. At the time of acute deterioration of HF or sudden onset of cardiac ischemia, patients often have congestion or elevation of LV end diastolic pressure. In such conditions, the immune system, neurohormonal factors such as TNFα and other cytokines are activated with concurrent activation of sympathetic nerve, all of which cause endothelial damage and other organ disorders [35]. In fact, acute MI is associated with a marked increase of inflammatory cells. Previous reports have demonstrated that inflammatory responses and neurohormonal factors cause the generation of oxidative stress not only from the myocardium but also from the vasculature [36–40]. These observations are consistent with our result showing that alteration of systemic ROS markers may not always reflect ROS generation in the myocardium.

Redox status estimated by in vivo ESR

ESR spectroscopy is a useful method to estimate redox status in living animals. In this study, we demonstrated using *in vivo* ESR spectroscopy that increased generation of free radicals in the heart correlated with dilatation of LV and decrease in EF, both of which are indices of the myocardial remodelling process after MI.

There are several advantages to determine ROS generation by *in vivo* ESR spectroscopy. First, the method allows non-invasive assessment of ROS generation in an *in vivo* setting. Secondly, *in vivo* ESR can be repeated in the same animal at different time points, indicating that the ESR technique has the potential to be used as a diagnostic tool in the future. Thirdly, this ESR technique can estimate and quantify the 'net' redox state. Antioxidant enzymes and reductants (such as glutathione) in the ROS generating system together determine the total redox status in biological systems, which may change dynamically and acutely in the heart after MI. Byproducts of free oxygen radicals such as lipid

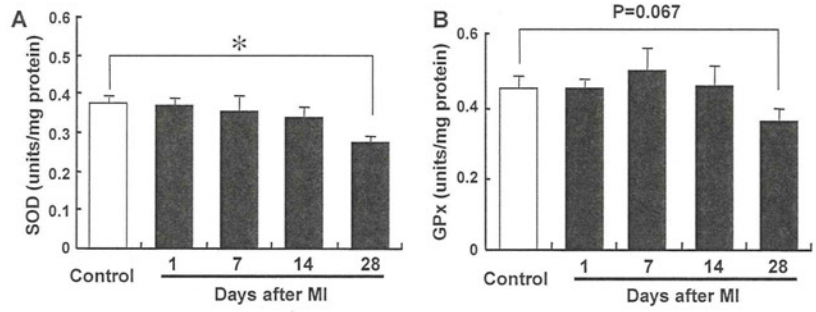

Figure 4. Time-dependent changes of activities of SOD (A) and GPx (B) in non-infarcted myocardium from sham-operated control ($n=7$) and on day 1 ($n=6$), day 7 ($n=10$), day 14 ($n=9$) and day 28 ($n=8$) after MI. Values are means ± SEM. * $p<0.05$ compared with sham-operated control.

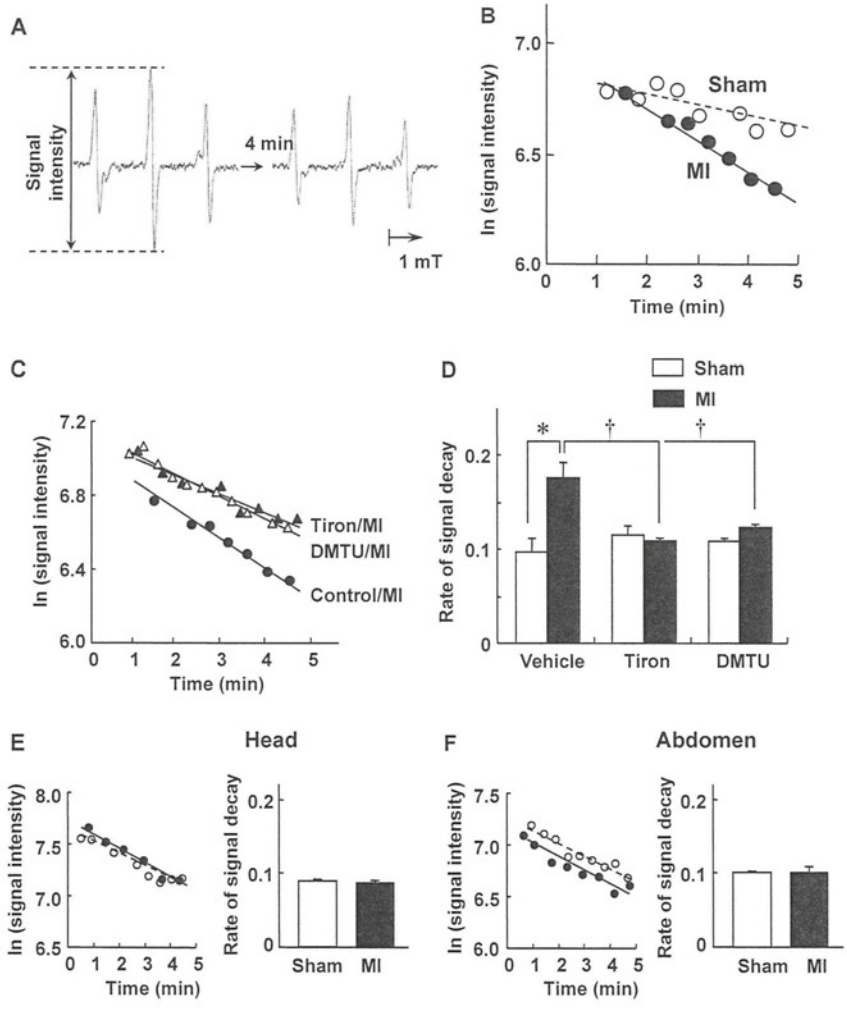

Figure 5. (A) A representative ESR signal of methoxycarbonyl-PROXYL at the chest level of a mouse with myocardial infarction (MI). (B) Semilogarithmic plots of the peak heights of the ESR spectra of methoxycarbonyl-PROXYL after spin probe injection. The signal intensity declined with time, which is defined as the signal decay. (C) The effects of addition of free radical scavengers on the rate of signal decay measured by *in vivo* ESR spectroscopy in individual MI mice. Tiron (a superoxide scavenger) or dimetylthiourea (DMTU; a hydroxyradical scavenger) was injected simultaneously with the injection of methoxycarbonyl-PROXYL. (D) Rates of signal decay measured by *in vivo* ESR in sham and MI groups in the absence and presence of radical scavengers ($n=6$ in each group). *$p<0.01$ vs sham-vehicle group and †$p<0.01$ vs MI-vehicle group. Values are means ± SEM. (E, F) Representative plots of individual mice and rates of *in vivo* ESR signal decay in sham and MI groups ($n=5$ each) measured at the head (E) and abdomen (F).

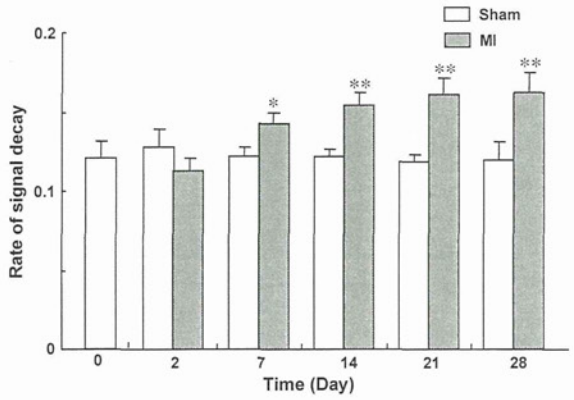

Figure 6. Changes in the rates of signal decay over time measured by *in vivo* ESR spectroscopy in sham and MI mice at days 0, 2, 7, 14 and 28 after operation ($n=7$ in each group). Values are means ±SEM. $*p<0.05$, $**p<.01$ vs sham values for the rate of signal decay.

peroxide, products of protein modifications and DNA damage do not always represent the net capacity of ROS reactions and do not necessary reflect ROS generation in specific organs or tissue. Difficulty in the interpretation of enhanced signal decay has been pointed out, because the nitroxyl radicals are known to react with not only free radicals but also other reductants including ascorbic acid and glutathione. However, we found that the increased ESR signal decay in heart failure was normalized by the addition of Tiron and DMTU. Furthermore, the TBARs study provided evidence that the ESR data reflect the increase of ROS in the failing heart, all of which support that the enhancement of signal decay in late remodelling represents at least the alteration of total redox status in the myocardium, most probably due to an increase of ROS.

Alteration of antioxidants and lipid peroxidation in non-infarct myocardium

We found that ROS markers including both byproducts of ROS and antioxidant enzymes were altered concomitantly in urine and blood at the early phase after MI and were normalized at the late remodelling state at 28 days post-MI. An increase of lipid peroxidation indicated by TBARS in infarct myocardium coincided with these systemic alterations (Figures 1 and 2). On the contrary, with the progression of remodelling represented by LV dilatation and reduced ejection fraction, the TBARS level in non-infarct myocardium increased at day 28. The immunohistochemical analysis by HEL antigen substantiated the finding that ROS was increased in the non-infarct myocardium during late remodelling. It is consistent with our previous findings in a tachycardia-induced canine HF model, in which ROS generation was enhanced in the failing myocardium and correlated with LV end-diastolic pressure and LV ejection fraction [41]. Nevertheless, it remains unknown why oxidative stress was not detectable in urine or in blood in late remodelling after MI, even with the progression of remodelling. A possible explanation is the differences in the source and amount of ROS between the early phase and the chronic phase of HF. In the later phase of post-MI remodelling, ROS increase may occur mainly in the myocardium and multiple defense mechanisms against ROS stabilize the levels in blood and urine. Moreover, ROS is so short-lived that it may not be possible to detect them in urine or blood when the source is localized in a single organ. In contrast, systemic inflammatory responses manifested clinically as leukocytosis and increased cytokines during acute deterioration or sudden ischemia [42–46] may not have enough time to cope with the acute ROS attack and redox change. We suspect that the acute increase in systemic ROS markers after MI is due to systemic activation of inflammatory cells. However, while administration of cyclophosphamide depletes leukocytes by 93% [15,47], the drug inhibited TBARS only partially by ~ 48% (data not shown). This indicates that sources other than leukocytes, such as vasculature, may contribute to systemic ROS generation in the acute phase of MI. All of these results suggest the difficulties of detecting ROS in blood or urine by specific markers in chronic HF, even with enhanced production of ROS from the remodelling myocardium.

Among the many detection techniques of ROS markers available currently, the most sensitive method is the detection of isoprostanes by mass spectroscopy. However, it is known that most of the major peaks of isoprostanes are not elevated in urine from HF patients [30]. Furthermore, commercially available ELISA kits are not as reliable as GC-MS assay [48]. Therefore, we measured a sensitive but not very specific marker TBARS for estimating ROS in plasma.

Clinical implications

Our study suggests that the increased local production of ROS is not always reflected in blood or urine during progression of remodelling. ROS are extremely unstable and difficult to detect directly. The establishment of a non-invasive method to detect ROS generated locally in the remodelling myocardium may permit time- and tissue-targeted therapy for more effective treatment of remodelling and failing heart.

Conclusion

We demonstrated that the generation of ROS in the non-infarct myocardium increases with the progression of cardiac remodelling and this increase is not

reflected by the levels of ROS markers in blood and urine. Clarification of the mechanisms of ROS-mediated remodelling and targeting non-infarct myocardium may lead to novel and effective therapeutic strategies for HF.

Acknowledgements

This study was supported in part by the Uehara memorial foundation and grants from the Ministry of Education (181-00006). A part of this study was conducted in Kyushu University Station for Collaborative Research II.

***Declaration of interest*:** The authors report no conflicts of interest. The authors alone are responsible for the content and writing of the paper.

References

[1] Gheorghiade M, Bonow RO. Chronic heart failure in the United States: a manifestation of coronary artery disease. Circulation 1998;97:282–289.

[2] Cohn JN, Ferrari R, Sharpe N. Cardiac remodeling—concepts and clinical implications: a consensus paper from an international forum on cardiac remodeling. Behalf of an International Forum on Cardiac Remodeling. J Am Coll Cardiol 2000;35:569–582.

[3] Liew CC, Dzau VJ. Molecular genetics and genomics of heart failure. Nat Rev Genet 2004;5:811–825.

[4] Tsutsui H, Ide T, Hayashidani S, Kinugawa S, Suematsu N, Utsumi H, Takeshita A. Effects of ACE inhibition on left ventricular failure and oxidative stress in Dahl salt-sensitive rats. J Cardiovasc Pharmacol 2001;37:725–733.

[5] Ichihara S, Yamada Y, Ichihara G, Kanazawa H, Hashimoto K, Kato Y, Matsushita A, Oikawa S, Yokota M, Iwase M. Attenuation of oxidative stress and cardiac dysfunction by bisoprolol in an animal model of dilated cardiomyopathy. Biochem Biophys Res Commun 2006;350:105–113.

[6] Mollnau H, Oelze M, August M, Wendt M, Daiber A, Schulz E, Baldus S, Kleschyov AL, Materne A, Wenzel P, Hink U, Nickenig G, Fleming I, Munzel T. Mechanisms of increased vascular superoxide production in an experimental model of idiopathic dilated cardiomyopathy. Arterioscler Thromb Vasc Biol 2005;25:2554–2559.

[7] Shite J, Qin F, Mao W, Kawai H, Stevens SY, Liang C. Antioxidant vitamins attenuate oxidative stress and cardiac dysfunction in tachycardia-induced cardiomyopathy. J Am Coll Cardiol 2001;38:1734–1740.

[8] Carlberg I, Mannervik B. Purification and characterization of the flavoenzyme glutathione reductase from rat liver. J Biol Chem 1975;250:5475–5480.

[9] Ide T, Tsutsui H, Kinugawa S, Suematsu N, Hayashidani S, Ichikawa K, Utsumi H, Machida Y, Egashira K, Takeshita A. Direct evidence for increased hydroxyl radicals originating from superoxide in the failing myocardium. Circ Res 2000;86:152–157.

[10] Lang D, Mosfer SI, Shakesby A, Donaldson F, Lewis MJ. Coronary microvascular endothelial cell redox state in left ventricular hypertrophy: the role of angiotensin II. Circ Res 2000;86:463–469.

[11] Kinugawa S, Tsutsui H, Hayashidani S, Ide T, Suematsu N, Satoh S, Utsumi H, Takeshita A. Treatment with dimethylthiourea prevents left ventricular remodeling and failure after experimental myocardial infarction in mice: role of oxidative stress. Circ Res 2000;87:392–398.

[12] Shiomi T, Tsutsui H, Matsusaka H, Murakami K, Hayashidani S, Ikeuchi M, Wen J, Kubota T, Utsumi H, Takeshita A. Overexpression of glutathione peroxidase prevents left ventricular remodeling and failure after myocardial infarction in mice. Circulation 2004;109:544–549.

[13] Matsushima S, Kinugawa S, Ide T, Matsusaka H, Inoue N, Ohta Y, Yokota T, Sunagawa K, Tsutsui H. Overexpression of glutathione peroxidase attenuates myocardial remodeling and preserves diastolic function in diabetic heart. Am J Physiol Heart Circ Physiol 2006;291:H2237–H2245.

[14] Suematsu N, Tsutsui H, Wen J, Kang D, Ikeuchi M, Ide T, Hayashidani S, Shiomi T, Kubota T, Hamasaki N, Takeshita A. Oxidative stress mediates tumor necrosis factor-alpha-induced mitochondrial DNA damage and dysfunction in cardiac myocytes. Circulation 2003;107:1418–1423.

[15] Machida Y, Kubota T, Kawamura N, Funakoshi H, Ide T, Utsumi H, Li YY, Feldman AM, Tsutsui H, Shimokawa H, Takeshita A. Overexpression of tumor necrosis factor-alpha increases production of hydroxyl radical in murine myocardium. Am J Physiol Heart Circ Physiol 2003;284:H449–H455.

[16] Foo RS, Siow RC, Brown MJ, Bennett MR. Heme oxygenase-1 gene transfer inhibits angiotensin II-mediated rat cardiac myocyte apoptosis but not hypertrophy. J Cell Physiol 2006;209:1–7.

[17] Nakagami H, Takemoto M, Liao JK. NADPH oxidase-derived superoxide anion mediates angiotensin II-induced cardiac hypertrophy. J Mol Cell Cardiol 2003;35:851–859.

[18] Siwik DA, Chang DL, Colucci WS. Interleukin-1beta and tumor necrosis factor-alpha decrease collagen synthesis and increase matrix metalloproteinase activity in cardiac fibroblasts *in vitro*. Circ Res 2000;86:1259–1265.

[19] Siwik DA, Pagano PJ, Colucci WS. Oxidative stress regulates collagen synthesis and matrix metalloproteinase activity in cardiac fibroblasts. Am J Physiol Cell Physiol 2001;280:C53–C60.

[20] Matsushima S, Ide T, Yamato M, Matsusaka H, Hattori F, Ikeuchi M, Kubota T, Sunagawa K, Hasegawa Y, Kurihara T, Oikawa S, Kinugawa S, Tsutsui H. Overexpression of mitochondrial peroxiredoxin-3 prevents left ventricular remodeling and failure after myocardial infarction in mice. Circulation 2006;113:1779–1786.

[21] Pimentel DR, Amin JK, Xiao L, Miller T, Viereck J, Oliver-Krasinski J, Baliga R, Wang J, Siwik DA, Singh K, Pagano P, Colucci WS, Sawyer DB. Reactive oxygen species mediate amplitude-dependent hypertrophic and apoptotic responses to mechanical stretch in cardiac myocytes. Circ Res 2001;89:453–460.

[22] Shiomi T, Tsutsui H, Hayashidani S, Suematsu N, Ikeuchi M, Wen J, Ishibashi M, Kubota T, Egashira K, Takeshita A. Pioglitazone, a peroxisome proliferator-activated receptor-gamma agonist, attenuates left ventricular remodeling and failure after experimental myocardial infarction. Circulation 2002;106:3126–3132.

[23] Yamamoto Y, Takahashi K. Glutathione peroxidase isolated from plasma reduces phospholipid hydroperoxides. Arch Biochem Biophys 1993;305:541–545.

[24] Sano H, Matsumoto K, Utsumi H. Synthesis and imaging of blood-brain-barrier permeable nitroxyl-probes for free radical reactions in brain of living mice. Biochem Mol Biol Int 1997;42:641–647.

[25] Han JY, Takeshita K, Utsumi H. Noninvasive detection of hydroxyl radical generation in lung by diesel exhaust particles. Free Radic Biol Med 2001;30:516–525.

[26] Phumala N, Ide T, Utsumi H. Noninvasive evaluation of *in vivo* free radical reactions catalyzed by iron using *in vivo* ESR spectroscopy. Free Radic Biol Med 1999;26:1209–1217.
[27] Belch JJ, Bridges AB, Scott N, Chopra M. Oxygen free radicals and congestive heart failure. Br Heart J 1991;65:245–248.
[28] Dieterich S, Bieligk U, Beulich K, Hasenfuss G, Prestle J. Gene expression of antioxidative enzymes in the human heart: increased expression of catalase in the end-stage failing heart. Circulation 2000;101:33–39.
[29] Ide T, Tsutsui H, Hayashidani S, Kang D, Suematsu N, Nakamura K, Utsumi H, Hamasaki N, Takeshita A. Mitochondrial DNA damage and dysfunction associated with oxidative stress in failing hearts after myocardial infarction. Circ Res 2001;88:529–535.
[30] Cargnoni A, Ceconi C, Bernocchi P, Boraso A, Parrinello G, Curello S, Ferrari R. Reduction of oxidative stress by carvedilol: role in maintenance of ischaemic myocardium viability. Cardiovasc Res 2000;47:556–566.
[31] Guo P, Nishiyama A, Rahman M, Nagai Y, Noma T, Namba T, Ishizawa M, Murakami K, Miyatake A, Kimura S, Mizushige K, Abe Y, Ohmori K, Kohno M. Contribution of reactive oxygen species to the pathogenesis of left ventricular failure in Dahl salt-sensitive hypertensive rats: effects of angiotensin II blockade. J Hypertens 2006;24:1097–1104.
[32] Miwa S, Toyokuni S, Nishina T, Nomoto T, Hiroyasu M, Nishimura K, Komeda M. Spaciotemporal alteration of 8-hydroxy-2′-deoxyguanosine levels in cardiomyocytes after myocardial infarction in rats. Free Radic Res 2002;36:853–858.
[33] Zhang GX, Kimura S, Nishiyama A, Shokoji T, Rahman M, Yao L, Nagai Y, Fujisawa Y, Miyatake A, Abe Y. Cardiac oxidative stress in acute and chronic isoproterenol-infused rats. Cardiovasc Res 2005;65:230–238.
[34] Li H, Lawson JA, Reilly M, Adiyaman M, Hwang SW, Rokach J, FitzGerald GA. Quantitative high performance liquid chromatography/tandem mass spectrometric analysis of the four classes of F(2)-isoprostanes in human urine. Proc Natl Acad Sci USA 1999;96:13381–13386.
[35] Agnoletti L, Curello S, Bachetti T, Malacarne F, Gaia G, Comini L, Volterrani M, Bonetti P, Parrinello G, Cadei M, Grigolato PG, Ferrari R. Serum from patients with severe heart failure downregulates eNOS and is proapoptotic: role of tumor necrosis factor-alpha. Circulation 1999;100:1983–1991.
[36] Kunsch C, Medford RM. Oxidative stress as a regulator of gene expression in the vasculature. Circ Res 1999;85:753–766.
[37] Al-Mehdi AB, Zhao G, Dodia C, Tozawa K, Costa K, Muzykantov V, Ross C, Blecha F, Dinauer M, Fisher AB. Endothelial NADPH oxidase as the source of oxidants in lungs exposed to ischemia or high K+. Circ Res 1998;83:730–737.
[38] Iuchi T, Akaike M, Mitsui T, Ohshima Y, Shintani Y, Azuma H, Matsumoto T. Glucocorticoid excess induces superoxide production in vascular endothelial cells and elicits vascular endothelial dysfunction. Circ Res 2003;92:81–87.
[39] Bertuglia S, Giusti A. Microvascular oxygenation, oxidative stress, NO suppression and superoxide dismutase during postischemic reperfusion. Am J Physiol Heart Circ Physiol 2003;285:H1064–H1071.
[40] Taniyama Y, Griendling KK. Reactive oxygen species in the vasculature: molecular and cellular mechanisms. Hypertension 2003;42:1075–1081.
[41] Aebi H. Catalase *in vitro*. Methods Enzymol 1984;105:121–126.
[42] Nakamura H, Takata S, Umemoto S, Matsuzaki M. Induction of left ventricular remodeling and dysfunction in the recipient heart following donor heart myocardial infarction: new insights into the pathological role of tumor necrosis factor-alpha from a novel heterotopic transplant-coronary ligation model. J Cardiol 2003;41:41–42.
[43] Maury CP. Monitoring the acute phase response: comparison of tumour necrosis factor (cachectin) and C-reactive protein responses in inflammatory and infectious diseases. J Clin Pathol 1989;42:1078–1082.
[44] Guillen I, Blanes M, Gomez-Lechon MJ, Castell JV. Cytokine signaling during myocardial infarction: sequential appearance of IL-1 beta and IL-6. Am J Physiol 1995;269:R229–R235.
[45] Basaran Y, Basaran MM, Babacan KF, Ener B, Okay T, Gok H, Ozdemir M. Serum tumor necrosis factor levels in acute myocardial infarction and unstable angina pectoris. Angiology 1993;44:332–337.
[46] Marx N, Neumann FJ, Ott I, Gawaz M, Koch W, Pinkau T, Schomig A. Induction of cytokine expression in leukocytes in acute myocardial infarction. J Am Coll Cardiol 1997;30:165–170.
[47] Fine PE. Implications of different study designs for the evaluation of acellular pertussis vaccines. Dev Biol Stand 1997;89:123–133.
[48] Pratico D, Lawson JA, Rokach J, FitzGerald GA. The isoprostanes in biology and medicine. Trends Endocrinol Metab 2001;12:243–247.

This paper was first published online on iFirst on 1 December 2008.

Annals of Biomedical Engineering, Vol. 37, No. 1, January 2009 (© 2008) pp. 82–93
DOI: 10.1007/s10439-008-9595-8

Computationally Managed Bradycardia Improved Cardiac Energetics While Restoring Normal Hemodynamics in Heart Failure

KAZUNORI UEMURA,[1] KENJI SUNAGAWA,[2] and MASARU SUGIMACHI[1]

[1]Department of Cardiovascular Dynamics, Advanced Medical Engineering Center, National Cardiovascular Center Research Institute, 5-7-1 Fujishirodai, Suita 565-8565, Japan; and [2]Department of Cardiovascular Medicine, Kyushu University Graduate School of Medical Sciences, Fukuoka 812-8582, Japan

(*Received 9 September 2008; accepted 29 October 2008; published online 12 November 2008*)

Abstract—In acute heart failure, systemic arterial pressure (AP), cardiac output (CO), and left atrial pressure (P_{LA}) have to be controlled within acceptable ranges. Under this condition, cardiac energetic efficiency should also be improved. Theoretically, if heart rate (HR) is reduced while AP, CO, and P_{LA} are maintained by preserving the functional slope of left ventricular (LV) Starling's curve (S_L) with precisely increased LV end-systolic elastance (E_{es}), it is possible to improve cardiac energetic efficiency and reduce LV oxygen consumption per minute (MVO_2). We investigated whether this hemodynamics can be accomplished in acute heart failure using an automated hemodynamic regulator that we developed previously. In seven anesthetized dogs with acute heart failure ($CO < 70$ mL min^{-1} kg^{-1}, $P_{LA} > 15$ mmHg), the regulator simultaneously controlled S_L with dobutamine, systemic vascular resistance with nitroprusside and stressed blood volume with dextran or furosemide, thereby controlling AP, CO, and P_{LA}. Normal hemodynamics were restored and maintained (CO; 88 ± 3 mL min^{-1} kg^{-1}, P_{LA}; 10.9 ± 0.4 mmHg), even when zatebradine significantly reduced HR ($-27 \pm 3\%$). Following HR reduction, E_{es} increased ($+34 \pm 14\%$), LV mechanical efficiency (stroke work/oxygen consumption) increased ($+22 \pm 6\%$), and MVO_2 decreased ($-17 \pm 4\%$) significantly. In conclusion, in a canine acute heart failure model, computationally managed bradycardia improved cardiac energetic efficiency while restoring normal hemodynamic conditions.

Keywords—Ventricular oxygen consumption, Mechanical efficiency, Specific bradycardic agent.

INTRODUCTION

Systemic arterial pressure (AP), cardiac output (CO), and left atrial pressure (P_{LA}) are three major variables necessary to guarantee survival. In the management of patients with acute heart failure following myocardial infarction or cardiac surgery, these variables have to be controlled within acceptable ranges.[1] Since the failing heart is in a critical state of myocardial energetics,[19] improvement of cardiac energetic efficiency is also essential in the management of such patients. Therapeutic interventions that enhance cardiac energetic efficiency have proven to be beneficial with respect to long-term outcome.[20] Reduction of heart rate (HR) has been shown to improve cardiac energetic efficiency.[6,26] However, in the failing heart, reduction of HR alone may decrease CO, and compromise hemodynamics.[5,13]

We previously demonstrated that AP, CO, and P_{LA} are determined by a mechanical equilibrium of the functional slope of Starling's curve (S_L) for the left ventricle (LV), systemic vascular resistance (R), and stressed blood volume (V).[30–32] Conversely, S_L, R, and V can be calculated from AP, CO, and P_{LA}, indicating that a set of AP, CO, and P_{LA} values uniquely corresponds to a set of S_L, R, and V values. When HR is reduced, the three variables of AP, CO, and P_{LA} can only be maintained by increasing LV contractility (LV end-systolic elastance, E_{es}) to offset HR reduction and to preserve S_L (see *Theoretical analysis* in "Materials and Methods"). In this hemodynamics, total mechanical energy of LV contraction, which is indicated by LV pressure–volume area (PVA), also increases with HR reduction. Increases in both E_{es} and PVA elevate LV oxygen consumption per beat (BVO_2).[28,29] However, since the increase in the external work done by LV is greater than the increase in BVO_2, cardiac energetic efficiency is improved. Furthermore, LV oxygen consumption per minute (MVO_2) decreases because the reduction in HR is sufficient to compensate for the increase in BVO_2.

To realize the above hemodynamics (optimal hemodynamics) in patients with acute heart failure, AP, CO, and P_{LA} should be controlled under HR

Address correspondence to Kazunori Uemura, Department of Cardiovascular Dynamics, Advanced Medical Engineering Center, National Cardiovascular Center Research Institute, 5-7-1 Fujishirodai, Suita 565-8565, Japan. Electronic mail: kuemura@ri.ncvc.go.jp

reduction by regulating infusions of multiple cardiovascular drugs such as inotropes and vasodilators. However, the control process is difficult and time-consuming, since the responses of AP, CO, and P_{LA} to these drugs vary between patients and within patient over time, and the responses are interrelated.[9,23] We previously demonstrated that it is possible to control AP, CO, and P_{LA} stably and accurately by directly controlling S_L, R, and V with cardiovascular drugs, due to their mechanical equilibrium.[30] This strategy is feasible because the responses of S_L to inotropes, R to vasodilators, and V to volume expander or diuretics are relatively invariable.[30] Furthermore, these three input–output relations; namely, inotrope–S_L, vasodilator–R, and volume expanders/diuretics–V are effectively decoupled. We hypothesized that this approach would be especially efficacious in accomplishing optimal hemodynamics in acute heart failure. Under HR reduction, an excessive increase in E_{es} will compromise the cardiac energetic efficiency.[15] Therefore E_{es} should be increased to a precise level. This can be done through a tight control of the inotrope–S_L relation. Although inotropes also affect R or V,[3,7] these effects can easily be compensated by the vasodilator–R and volume expanders/diuretics–V relations.

The purpose of this study was to prove the hypothesis that direct control of S_L, R, and V under HR reduction attains the optimal hemodynamics and at the same time improves cardiac energetic efficiency and reduces MVO_2 in a canine model of acute heart failure, as predicted in *Theoretical Analysis*. An automated hemodynamic regulator that we developed previously[30] was used to directly control S_L, R, and V. The regulator directly controls S_L with dobutamine (DOB), R with sodium nitroprusside (SNP), and V with dextran (DEX) and furosemide (FUR), thereby controlling AP, CO, and P_{LA}. To reduce HR, we used a specific bradycardic agent, zatebradine (UL-FS49) that specifically reduces HR without affecting LV contractility.[12,24]

MATERIALS AND METHODS

Theoretical analysis

S_L is theoretically determined by E_{es}, HR, R, and diastolic myocardial stiffness (k), and can be expressed by the following formula[31]:

$$S_L = \frac{1}{k} \cdot \frac{E_{es}}{(E_{es}/HR) + R} \tag{1}$$

Equation (1) can be rewritten as follows:

$$E_{es} = \frac{S_L \cdot k \cdot R}{1 - S_L \cdot k/HR} \tag{2}$$

The external work done by LV is represented by stroke work (SW) and expressed as[11]

$$SW = (P_{es} - P_{ed}) \cdot CO/HR \tag{3}$$

where P_{es} is LV end-systolic pressure and P_{ed} is end-diastolic pressure. In the LV pressure–volume diagram, PVA is the area circumscribed by the end-systolic pressure volume relation, the end-diastolic pressure volume relation, and the systolic pressure volume trajectory of LV. PVA, an index of total mechanical energy of LV contraction, is the sum of potential energy and external work of LV,[28,29] and can be expressed as

$$PVA = P_{es} \cdot P_{es}/2E_{es} + SW \tag{4}$$

If we approximate P_{es} to AP and P_{ed} to P_{LA}, SW and PVA can be expressed as

$$SW = (AP - P_{LA}) \cdot CO/HR \tag{5}$$

$$PVA = AP \cdot AP/2E_{es} + SW \tag{6}$$

BVO_2 is related to PVA and E_{es} as follows[28,29]:

$$BVO_2 = \alpha \cdot PVA + \beta \cdot E_{es} + \gamma \tag{7}$$

where α, β, and γ are constants representing oxygen cost of PVA, oxygen cost of contractility, and basal metabolism, respectively. MVO_2 is expressed as follows:

$$MVO_2 = BVO_2 \cdot HR \tag{8}$$

Using Eqs. (2–8) and fixed values of AP, CO, and P_{LA} (Table 1), we numerically simulated the individual relations of HR with E_{es}, SW, PVA, BVO_2, LV mechanical efficiency (ME) and MVO_2 (Fig. 1). In these computations, representative k, α, β, and γ values (Table 1) were used, which are appropriate for a 20-kg dog.[10,29] In Eq. (2), S_L was calculated from the ratio of CO to logarithmic function of P_{LA} as described

TABLE 1. Values of the parameters used in *Theoretical Analysis*.

Parameters	Values
AP, mmHg	100
CO, mL min^{-1} kg^{-1}	100
P_{LA}, mmHg	10
k, mL^{-1}	0.082
α, mL O_2 · mmHg^{-1} · mL^{-1}	1.8×10^{-5}
β, mL O_2 · beat^{-1} · mmHg^{-1} · mL	0.0018
γ, mL O_2 · beat^{-1}	0.01

AP, systemic arterial pressure; CO, cardiac output; P_{LA}, left atrial pressure; k, left ventricular diastolic myocardial stiffness; α, oxygen cost of pressure–volume area; β, oxygen cost of contractility; γ, constant representing basal metabolism.